Chapter 7
Structural and Optical Characterization of ZrO_2 and Y_2O_3-ZrO_2 Nanopowders

Nadiia Korsunska, Anton Zhuk, Vasyl Papusha, Oleksandr Kolomys, Yuliya Polishchuk, Yurii Bacherikov, Viktor Strelchuk, Vasyl Kladko, Tetyana Konstantinova, Tetyana Kryshtab, and Larysa Khomenkova

Abstract Structural and optical properties of pure and Y-doped ZrO_2 nanopowders with different Y content sintered by co-precipitation of Zr and Y nitrates were investigated. It was observed that the increase of Y content stimulates the transformation of crystalline phase from monoclinic through tetragonal to cubic while the increase of calcinations time leads to the increase of ZrO_2 grain sizes. Generally, room temperature photo- and cathodoluminescence spectra showed several bands in blue–orange range. The increase of powder grains results in the enhancement of 2.81-eV photoluminescence caused probably by volume centers. Besides blue–orange emission, additional "red" cathodoluminescence band was observed. Its intensity exceeds essentially the magnitude of other components and increases with cooling. This "red" band was found to be complex and caused by intradefect transition. The excitation mechanism of this band is discussed.

Keywords Y-doped ZrO_2 • Luminescence • Raman scattering • TEM • Structural and optical characterization

N. Korsunska • A. Zhuk • V. Papusha • O. Kolomys • Y. Polishchuk • Y. Bacherikov
V. Strelchuk • V. Kladko • L. Khomenkova (✉)
V. Lashkaryov ISP of NAS of Ukraine, 45 Pr. Nauky, Kyiv 03028, Ukraine
e-mail: khomen@ukr.net

T. Konstantinova
Donetsk Institute for Physics and Engineering named after O.O. Galkin of the NASU,
72 R. Luxemburg str., Donetsk 83114, Ukraine
e-mail: matscidep@aim.com

T. Kryshtab
Department of Physics, ESFM-IPN, 07738 México D.F., México
e-mail: kryshtab@gmail.com

R. Pérez Campos et al. (eds.), *Materials Characterization*,
DOI 10.1007/978-3-319-15204-2_7

7.1 Introduction

Zirconia (ZrO_2) has attracted considerable attention because of its mechanical, electric, thermal, and luminescent properties. Emitting ZrO_2 allows different applications, for example, for oxygen sensor [1], laser techniques, biological labelling [2], thermoluminescent UV dosimeters, etc. Many different defect-related emission bands can be observed in pure and/or Y-stabilized ZrO_2 materials in visible spectral range [3, 4] that offer also an application of zirconia for white light emitting devices [5] and for a visualization of high energy radiation [6].

One of the methods to investigate the availability of ZrO_2 to such an application is the study of its cathodoluminescence (CL) which is not well addressed. Only a few works are devoted to CL investigation demonstrating different results [7, 8]. This can be due to different microstructure (type of crystalline lattice, size distribution of ZrO_2 grains, and different nature of radiative defects) of ZrO_2 materials that depends on the fabrication approach. In particular, freestanding ZrO_2 nanocrystals with different sizes, studied in [9], exhibit the lowest CL intensity for the smallest size nanocrystals.

In the present work ZrO_2 and Y_2O_3-ZrO_2 nanopowders with different Y content were investigated by means of Raman scattering, transmission electron microscopy (TEM), photo- (PL) and cathodoluminescence (CL) methods. The effect of fabrication parameters on material crystalline structure and light emission parameters as well as the difference in PL and CL spectra of the same powders were observed. The nature of emission centers and the mechanisms of their excitation are discussed.

7.2 Experimental

Undoped and doped nanopowders were synthesized by a co-precipitation technique from using $ZrOCl_2 \cdot nH_2O$ and $Y(NO_3)_3 \cdot nH_2O$ salts. The 25 % NH_4OH water solution was used as precipitant. Sediments were mixed for 1 h at room temperature at pH = 9. After this, they were repeatedly washed, filtered with distilled water and then the hydrogel was dried in a microwave furnace and calcined at 700 °C for $t_c = 1$ or 2 h. More details can be found elsewhere [10, 11].

Elemental analysis of powders investigated was performed by means of X-ray fluorescent method using EXPERT 3L W144U setup. Pure ZrO_2 ($t_c = 1$ h) and Y-doped ZrO_2 (ZYO) powders with 10 at% of Y content ($t_c = 1$ (ZYO-10-1) and 2 h (ZYO-10-2)) as well as with 15 at% of Y content ($t_c = 1$ h (ZYO-15)) were examined. Note that all the samples contained Fe and Zn as impurities.

Micro-Raman scattering spectra were detected using a Horiba Jobin T-64000 Raman spectrometer. A 488-nm line of Ar laser was used as the excitation source. The laser power was kept below 5 mW to prevent laser heating of sample investigated. XRD data were collected using ARL X'TRA powder diffractometer with CuKα wavelength ($\lambda = 0.15418$ nm) and grazing geometry ($\omega \sim 0.5°$). TEM observation was performed with JEOL JEM 200A instrument. For more details, see [12].

Photoluminescence (PL) was excited by 337-nm light of N_2-laser. In cathodoluminescence (CL) measurements the samples were excited by scanning electron beam in quasi-continuous regime at accelerating voltage $E = 75$ kV and current value (I) varied in the range 10–120 μA. PL and CL light was dispersed by grating monochromator and registered by PMT tube. CL was detected at 300 and 77 K, while PL was recorded at 300 K.

7.3 Results and Discussion

7.3.1 Structural Properties

ZrO_2 can exist in the three structural phases: monoclinic (m-ZrO_2), tetragonal (t-ZrO_2), and cubic (c-ZrO_2). At room temperature the m-ZrO_2 phase is stable [13], whereas both t-ZrO_2 and c-ZrO_2 phases can be stabilized by doping with bivalent or trivalent atoms, in particular with Y.

Figure 7.1a represents Raman scattering spectra of samples investigated. Pure ZrO_2 powder demonstrates multiple narrow phonon bands which correspond to nine A_g modes at 98, 175, 187, 302, 344, 473, 553, 633, and 706 cm^{-1}, and six B_g modes at 219, 330, 378, 499, 533, and 610 cm^{-1} which correspond to ZrO_2 monoclinic phase [14].

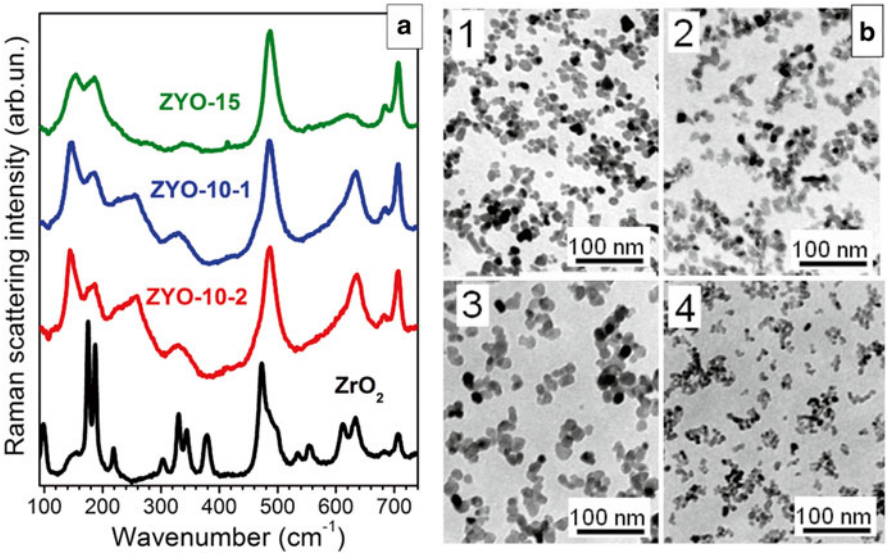

Fig. 7.1 (**a**) Raman spectra of undoped ZrO_2 and yttrium-doped samples (ZYO-10-1, ZYO-10-2 and ZYO-15). Spectral intensities have been normalized to their maximum value. For clarity, the spectra have been shifted in vertical direction. $E_{exc} = 2.54$ eV, (**b**) bright-field TEM images of pure ZrO2 (1), ZYO-10-1 (2), ZYO-10-2 (3) and ZYO-15 (4)

The ZYO-10-1 and ZYO-10-2 samples show broad bands peaked at 145, 259, 330, 612 and 636 cm^{-1} attributed to the modes of t-ZrO_2, small peaks at 175 and 187 cm^{-1} attributed to A_g modes m-ZrO_2 phase. Besides, several broad bands with the peak positions corresponding to m-ZrO_2 are also observed in these spectra that can be an evidence of a partial transformation of m-ZrO_2 and a coexistence of both t- and m-ZrO_2 phases (Fig. 7.1a). The band peaked at 259 cm^{-1} is not observed either for monoclinic or cubic phase [15] and can be exclusively assigned to the E_g mode of t-ZrO_2 [16]. The peak's broadening could be due to structural distortion. For ZYO-15 sample the peaks at 155, 279, and 618 cm^{-1} corresponded to c-phase were observed [17]. However, the peak at 485 cm^{-1} is detected also. Therefore, this sample can be considered as superposition of cubic and tetragonal phases with main contribution of cubic one. Observed transformation of crystallite structure is in agreement with XRD data obtained for the same samples and described in detail in [18].

Bright-field TEM images of samples investigated are shown in Fig. 7.1b. It is seen that the powders obtained by co-precipitation technique are single crystals with soft and easily destroyed agglomerates that are important for their successful application. From the analysis of crystal size distribution the mean sizes of nanocrystals were found to be $d = 12$ nm for pure ZrO_2 sample, $d = 11$ nm for ZYO-10-1 sample, and $d = 20$ nm for ZYO-10-2 sample as well as $d = 10$ nm for ZYO-15 sample. Thus, the increase of Y content stimulates the decrease of nanocrystal sizes, whereas the increase of calcination time results in their enlargement.

7.3.2 Light Emitting Properties

PL spectra of the samples with different Y content are shown in Fig. 7.2. They contain wide structural band in the region of 2.25–3.10 eV (400–550 nm) and the shoulder in the range of 2.06–2.17 eV (570–600 nm). The observed PL band can be approximated by three Gaussian-like components with maxima positions at ~2.81 eV (440 nm), ~2.43 eV (510 nm) and ~2.11 eV (587 mn) (dashed curves). The shape of PL spectra slightly depends on Y content in the samples calcinated for 1 h. The increase of calcination time in the samples with the 10 at% Y content resulted in the increase of the grain size from 11 to 20 nm leads to the high-energy shift of PL maximum due to increase of high-energy component contribution to PL spectra. At the same time the PL components peaked at ~2.11 eV (587 nm) and 2.43 eV (510 nm) are more pronounced in the sample with the small grain size. It should be noted that PL intensity did not vary considerably in all samples investigated.

CL spectra of samples measured at 300 K demonstrate two broad bands with maxima positions at 2.9 eV (425 nm) and 1.74 (700 nm) (blue and red bands) (Fig. 7.3). The intensity of red band exceeds essentially the intensity of blue one. The latter has a long-wavelength tail testifying to its non-elementary. Similar complex

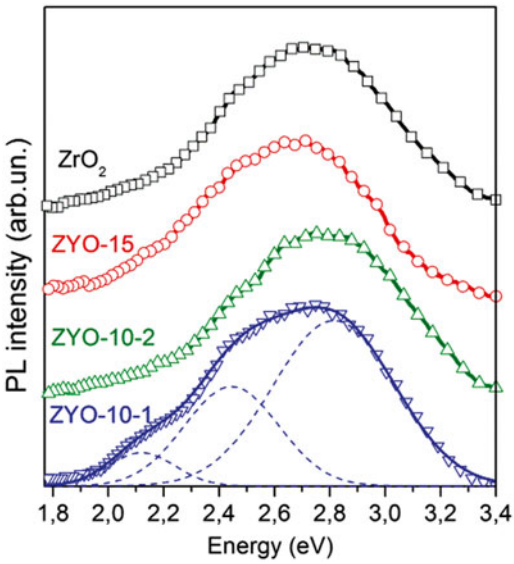

Fig. 7.2 PL spectra of pure ZrO_2 and ZYO powders. *Dashed curves* represent the approximation of PL spectrum of ZYO-10-1 sample by Gaussian-like components

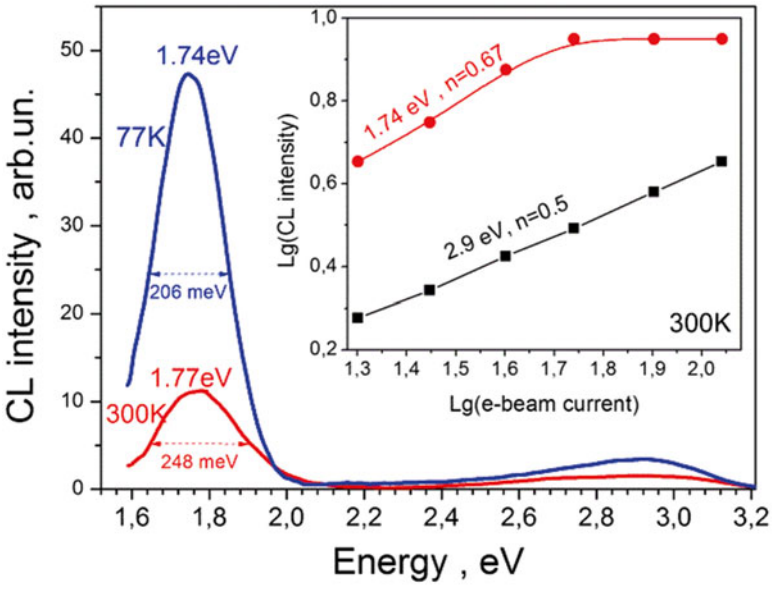

Fig. 7.3 CL spectra of ZYO powders measured at 300 and 77 K at $E = 75$ kV and $I = 120$ μA. The inset shows the variation of CL intensity for different CL bands (1.74 and 2.9 eV) versus e-beam current at 300 K

band was often observed in photo- [9], X-ray, and cathodoluminescence spectra [7], but the red band, to author's knowledge, was not earlier detected.

The cooling to 77 K enhances the intensity of both bands, but the red band increases mainly. Thus, the both bands show the thermal quenching in the range 77–300 K. Besides, the cooling results in the shift of red band peak position to lower energy side and in the decrease of its full width at half maximum (FWHM) (Fig. 7.3). Therefore we can conclude that it is also not elementary and with temperature decrease its low energy component increases mainly.

The variation of CL band intensities with electron beam current value plotted in log–log scale shows that the dependence for blue band can be approximated by a straight line in the whole range of applied current values, while the red band intensity saturates at $I > 55$ μA (Fig. 7.3 (inset)). The slopes of linear parts of these dependencies are lower than 1.

Under band-to-band excitation, the sub-linearity ($n < 1$) and subsequent saturation can be observed when the filling of emission centers by nonequilibrium carriers approaches to the center concentration [19]. Thus, we can suppose that this case is realized in our CL experiments.

As Fig. 7.2 shows, the PL spectra of all the samples investigated recorded under the excitation below band gap consist of several overlapped PL bands similarly to other data obtained on pure and Y-stabilized ZrO_2 [3, 5, 20]. The observed PL bands are usually ascribed to different intrinsic defects such as singly charged oxygen vacancies (F-centers) in the volume of nanocrystals or at their surface [3], as well as Zr^{3+} centers [20] or the different complexes including oxygen vacancies or distortion of crystal lattice due to these vacancies [3, 4].

Invariance of PL spectra shape on the Y content in our samples calcinated during 1 h testifies to the presence of the same defects with nearly the same concentration. At the same time the increase of calcination time resulted in the increase of crystallite sizes leads to the redistribution of PL component intensities. The formation of larger grains is accompanied by the decrease of their surface/volume ratio. This can be the reason of the increase of the contribution of 2.81-eV PL component and decrease of the intensities of 2.11 and 2.43 eV PL components. Thus, the former PL component can be ascribed to the volume defects (for instance, F-like center). This is in an agreement with the conclusion of [5, 21], where similar PL emission was attributed to grain volume defects. At the same time, the 2.11 and 2.43-eV PL components are more pronounced for the samples with smaller grains (Fig. 7.2) that allows attributing them to the grain surface defects. This is in accordance with the data of [7] where the 2.17-eV PL component which is close to that observed in our spectra (Fig. 7.2) was ascribed to defect states at the grain boundaries [3]. At the same time the band at ~2.48 eV (closed to 2.43 eV) was attributed to volume intrinsic defects—Zr^{3+} centers [20].

In CL spectra the blue band peak position is closed to that of high-energy PL component. It means obviously that the same defects are activated under intrinsic and extrinsic excitation light. However, under band-to-band excitation other defect can also be excited resulting in appearance of additional bright emission band in red spectral range.

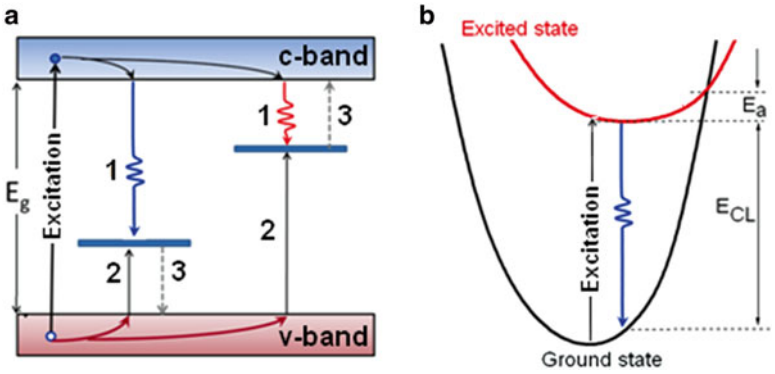

Fig. 7.4 (**a**) Simplified schema of electron transitions in the case of one-level radiative centers. The labels correspond to capture of free electrons (1) and free holes (2), as well as thermal escape of electrons or holes (3). *Undulating arrows* correspond to radiative transitions. (**b**) The coordination diagram showing the correspondence between excitation, radiative (E_{CL}), and nonradiative recombination in two-level center (intradefect transition). The E_a is the activation energy of thermal quenching of emission

As it was mentioned above, both observed CL bands show the thermal quenching above 77 K. Its low temperature range implies that activation energy (E_a) of quenching process cannot be high. Based on the comparison with data of [5], we could assume that $E_a \sim 0.2$–0.4 eV.

The thermal quenching can be caused, in general, by two processes (Fig. 7.4). One of them is the escape of electron (hole) into conduction (valence) band and its subsequent capture by nonradiative centers (external quenching) (Fig. 7.4a). Another one is the competition between radiative and nonradiative electron transitions in the same center (intrinsic quenching) (Fig. 7.4b).

The E_a value for external quenching is equal to the distance between the energy level of emission center and nearest permitted band [5]. If the internal quenching takes place, the E_a is the barrier between minimum of potential curve (configuration-coordinate diagram) of excited state and intersection point of potential curves of excited and ground states (Fig. 7.4b). However, irrespectively of quenching mechanism, we can conclude that the recombination center responsible for red emission has, at least, two levels (excited and ground states) because $E_a + E_{CL} < E_g$. Thus, red CL emission is caused by intradefect transition.

Radiative intradefect transition in visible range can be realized in some impurities as well as in the intrinsic defects (oxygen vacancies or Zr^{3+}). Currently, the latter emission mechanism is generally accepted for luminescence band(s) in ZrO_2. Taking into account the presence of Zn and Fe impurities in our powders, we think that the red CL emission can be caused by intradefect transition either in the impurity or in oxygen vacancies located nearby the impurity.

It is worth to note that this red emission was not detected either under light excitation (whatever excitation light energy below 6.0 eV in our experiment) or

under X-ray excitation (with 80 eV energy). Since red emission is the most efficient in CL spectra while the blue band can be stimulated by optical and X-ray excitation, one can conclude that red emitting centers require high-energy electrons to be excited and the main excitation mechanism is impact ionization. Indeed the number of hot electrons in CL experiment is much higher than in X-ray beam.

7.4 Conclusions

Luminescence and structural properties of Y_2O_3-doped ZrO_2 nanopowders sintered by co-precipitation of Zr and Y nitrates with different Y_2O_3 content were investigated by Raman scattering, TEM, photo- and cathodoluminescent methods. It was found that at constant calcination temperature, the Y content controls the change of crystalline phase. PL spectra of the samples consist of several overlapped bands in visible spectral range (at ~440, 510 and 560 nm). The contribution of all components to PL spectra does not depend on Y content, but it is affected by calcination time (powder grain sizes). Besides the bands observed in PL spectra, CL ones show additional "red" band which intensity exceeds essentially the magnitude of other CL components. At lower temperatures, preferable enhancement of "red" CL band, its narrowing and peak position shift to the longer wavelengths were found. This behavior testifies to the complexity of "red" CL band which nature and excitation mechanisms are discussed. The dominant contribution of red emission into CL spectra opens some perspectives for its application as a marker for high-energy radiation.

Acknowledgments This work is supported by the National Academy of Sciences of Ukraine (project III-4-11).

References

1. Fidelus JD, Lojkowski W, Millers D, Smits K, Grigorjeva L (2009) Advanced nanocrystalline ZrO_2 for optical oxygen sensors. IEEE Sensors 9:1268–1272
2. Jia R, Yang W, Bai Y, Li T (2004) Upconversion photoluminescence of ZrO_2:Er^{3+} nanocrystals synthesized by using butadinol as high boiling point solvent. Opt Mater 28:246–249
3. Nakajima H, Mori T (2006) Photoluminescence excitation bands corresponding to defect states due to oxygen vacancies in yttria-stabilized zirconia. J Alloys Compd 408–412:728–731
4. Smits K, Grigorjeva L, Millers D, Sarakovskis A, Grabis J, Lojkowski W (2011) Intrinsic defect related luminescence in ZrO_2. J Lumin 131:2058–2062
5. Petrik NG, Tailor DP, Orlando TM (1999) Laser-stimulated luminescence of yttria-stabilized cubic zirconia crystals. J Appl Phys 85:6770–6776
6. Kirm M, Aarik J, Sildos I (2005) Thin films of HfO_2 and ZrO_2 as potential scintillators. Nucl Instrum Meth Phys Res A 537:251–255
7. Smits K, Millers D, Grigorjeva L, Fidelus JD, Lojkowski W (2007) Comparison of ZrO_2:Y nanocrystals and macroscopic single crystal luminescence. J Phys: Conf Ser 93:012035

8. Ken Yueh H, Cox B (2003) Luminescence properties of zirconium oxide films. J Nucl Mater 323:57–67
9. Ramos-Brito F, Garcıa-Hipolito M, Martınez-Martinez R, Martinez-Sanchez E, Falcony C (2004) Preparation and characterization of photoluminescent praseodymium-doped ZrO_2 nanostructured powders. J Phys D: Appl Phys 37:L13–L16
10. Konstantinova T, Danilenko I, Glazunova V, Volkova G, Gorban O (2011) Mesoscopic phenomena in oxide nanoparticles systems: processes of growth. J Nanopart Res 13:4015–4023
11. Konstantinova T, Danilenko I, Varyukhin V (2013) Effects of surface and interface in oxide nanoparticle system. Springer Proc Phys 146:135–144
12. Doroshkevich AS, Danilenko IA, Konstantinova TE, Volkova GK, Glazunova VA (2010) Structural evolution of zirconia nanopowders as a coagulation process. Crystallogr Rep 55:863–865
13. Kontoyannis CG, Orkoula M (1994) Quantitative determination of the cubic, tetragonal and monoclinic phases in partially stabilized zirconias by Raman spectroscopy. J Mater Sci 29:5316–5320
14. Anastassakis E, Papanicolaou B, Asher IM (1975) Lattice dynamics and light scattering in hafnia and zirconia. J Phys Chem Solids 36:667–676
15. Nomura K, Mizutani Y, Kawai M, Nakamura Y, Yamamoto O (2000) Aging and Raman scattering study of scandia and yttria doped zirconia. Solid State Ionics 132:235–239
16. Shi L, Tin KC, Wong NB (1999) Thermal stability of zirconia membranes. J Mater Sci 34:3367–3374
17. Gazzoli D, Mattei G, Valigi M (2007) Raman and X-ray investigations of the incorporation of Ca^{2+} and Cd^{2+} in the ZrO_2 structure. J Raman Spectrosc 38:824–831
18. Korsunska N, Baran M, Zhuk A, Polischuk Y, Stara T, Kladko V, Bacherikov Y, Venger Z, Konstantinova T, Khomenkova L (2014) Role of paramagnetic defects in light emission processes in Y-doped ZrO_2 nanopowder. Mater Res Express 1:045011
19. Lashkarev VE, Lyubchenko AV, Sheinkman MK (1981) Non-equilibrium processes in photoconductors. Naukova dumka, Kyiv
20. Orera VM, Merino RI, Chen Y, Cases R, Alonso PJ (1990) Intrinsic electron and hole defects in stabilized zirconia single crystals. Phys Rev B 42:9782–9789
21. Lin C, Zhang C, Lin J (2007) Phase transformation and photoluminescence properties of nanocrystalline ZrO_2 powders prepared via the Pechini-type sol–gel process. J Phys Chem C 111:3300–3307